

# Exact new mobility edges between critical and localized states

Xin-Chi Zhou,<sup>1,\*</sup> Yongjian Wang,<sup>2,\*</sup> Ting-Fung Jeffrey Poon,<sup>1,\*</sup> Qi Zhou,<sup>3,†</sup> and Xiong-Jun Liu<sup>1,4,5,‡</sup>

<sup>1</sup>*International Center for Quantum Materials, School of Physics, Peking University, Beijing 100871, China*

<sup>2</sup>*School of Mathematical Sciences, Laboratory of Mathematics and Complex Systems,*

*MOE, Beijing Normal University, 100875 Beijing, China*

<sup>3</sup>*Chern Institute of Mathematics and LPMC, Nankai University, Tianjin 300071, China*

<sup>4</sup>*CAS Center for Excellence in Topological Quantum Computation,*

*University of Chinese Academy of Sciences, Beijing 100190, China*

<sup>5</sup>*International Quantum Academy, Shenzhen 518048, China*

The disorder systems host three types of fundamental quantum states, known as the extended, localized, and critical states, of which the critical states remain being much less explored. Here we uncover a novel type of exactly solvable mobility edges (MEs) separating localized states from robust critical states, and propose experimental realization. Here the robustness refers to the stability against both single-particle perturbation and interactions. The new MEs are exactly solved from a one-dimensional model, where both hopping coefficients and on-site potential are in a quasiperiodic mosaic manner. The analytic results enable us to *unambiguously* obtain the critical states which otherwise require arduous numerical verification including the careful finite size scalings. We further investigate the proposed model in the presence of perturbation and interactions, and show the robustness of the new MEs. The robustness of critical zones is protected by zeros of hopping coefficients in the thermodynamics limit. Finally, we propose a novel experimental scheme to realize the exactly solvable model and the new MEs in Rydberg array. This work may pave a way to precisely explore the critical states and new ME physics with experimental feasibility.

**Introduction.**—Anderson localization (AL) is a fundamental and ubiquitous quantum phenomenon that quantum states are exponentially localized without diffusion due to disorder [1]. Scaling theory shows that the all noninteracting states are localized in one and two dimensions with arbitrarily small disorder strength [2, 3], while in three dimension (3D), the localized and extended states can coexist at finite disorder strength, and be separated by a critical energy  $E_c$ , dubbed the mobility edge (ME). The ME leads to various fundamental phenomena, such as metal-insulator transition by varying the particle number density or the disorder strength [4]. Moreover, a system with ME exhibits strong thermoelectric response, enabling application in thermoelectric devices [5–7]. An important feature of ME between extended and localized states is that it is a stable phenomenon, and can survive under perturbations and interactions [8–12].

Unlike in randomly disordered system, the extended-AL transition and ME can be obtained in 1D system with quasiperiodic potential [13–28]. This result has triggered a lot of experimental studies in realizing quasiperiodic systems with ultracold atoms [29–33] and other synthetic systems, such as photonic crystals, optical cavities, and superconducting circuits [34–38]. More importantly, quasiperiodic systems can host a third type of states called critical states [39–43]. The critical states are extended but non-ergodic, locally scale-invariant and fundamentally different from the localized and extended states in spectral statistics [44–46], multifractal properties [47–49], and dynamical evolution [50–52]. With interaction between particles, the single-particle critical states may become many-body critical (MBC) phase [26, 53, 54] that interpolates the thermal and many-body localized phase [55, 56]. However, unlike localized and extended states, to confirm critical states is more subtle and requires arduous numerical calculations like finite-size

scaling, so it is highly important to develop exactly solvable models which can *unambiguously* determine critical states. Moreover, similar to the ME separating extended from localized states, can a new ME be obtained separating critical states from localized ones [24], in particular, in experimentally feasible models? A definite answer to this fundamental question is yet elusive but may be provided by resolving the following issues. First, one can develop an analytic model with exactly solvable ME between the critical states and localized ones. Further, one needs to confirm that such new ME is robust, e.g. in the presence of perturbation and/or interactions. Finally, the exactly solvable model with the new ME is feasible in experimental realization.

In this work, we propose an exactly solvable 1D model featured with mosaic type quasiperiodic hopping coefficients and on-site potential, and obtain unambiguously critical states and robust exact MEs. Not only the ME, but also the localization and critical features of all quantum states in the spectra are precisely determined by Avila’s global theory [57], enabling an accurate characterization of the critical states and the new MEs. We further confirm the robustness of MEs in the presence of single-particle perturbation and interactions. The robustness is rooted in a generic mechanism unveiled with our exactly solvable model to realize critical states. Finally, we propose a novel scheme with experimental feasibility to realize and detect the exact MEs based on an incommensurate Raman superarray of Rydberg atoms.

**Model.**—We propose the quasiperiodic mosaic models as pictorially shown in Fig. 1, which is described by

$$H = \sum_j (t_j a_j^\dagger a_{j+1} + \text{h.c.}) + \sum_j V_j n_j, \quad (1)$$

where the key ingredients are that both the quasiperiodic hop-

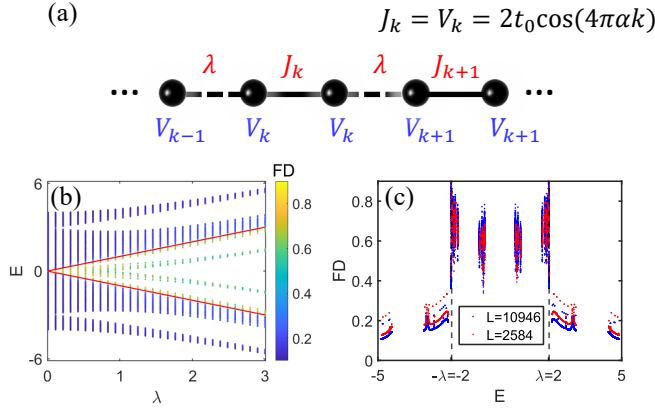


Figure 1. (a) The 1D quasiperiodic mosaic model. The black solid and dashed lines denote the quasiperiodic hopping  $J_k$  and constant hopping  $\lambda$ , respectively. The black sphere denotes a lattice site, and  $V_k$  is the quasiperiodic mosaic chemical potential. Here  $\alpha$  is an irrational number and  $k$  is an integer. (b) Fractal dimension (FD) of different eigenstates as a function of corresponding energies  $E$  and strength of mosaic potential  $\lambda$  for  $L = 2584$ . The red lines denote the mobility edges  $E_c = \pm\lambda$ . (c) FD versus energies  $E$  with fixed  $\lambda = 2.0$  for  $L = 2584$  (red dots) and  $L = 10946$  (blue dots). The dashed lines represent the MEs  $E_c = \pm\lambda$ . The  $t_0$  is set to 1 as energy unit.

pling coefficient  $t_j$  and on-site potential  $V_j$  are mosaic, with

$$\{t_j, V_j\} = \begin{cases} \{\lambda, 2t_0 \cos[2\pi\alpha(j-1) + \theta]\}, & j = 1 \bmod 2, \\ 2t_0 \cos(2\pi\alpha j + \theta)\{1, 1\}, & j = 0 \bmod 2, \end{cases} \quad (2)$$

the particle number operator  $n_j = a_j^\dagger a_j$ , with  $a_j^\dagger (a_j)$  the creation (annihilation) operator at site  $j$ , and  $\lambda$  and  $\theta$  denote hopping coefficient and phase offset, respectively. We take for convenience  $t_0 = 1$ , and set  $\theta = 0$  and  $\alpha = \lim_{n \rightarrow \infty} (F_{n-1}/F_n) = (\sqrt{5} - 1)/2$  without affecting generality, with  $F_n$  being Fibonacci numbers. For finite system one may choose the system size  $L = F_n$  and  $\alpha = F_{n-1}/F_n$  to impose the periodic boundary condition for numerical diagonalization of the tight-binding model in Eq. (1). We shall prove that the model has exact energy-dependent MEs separating localized states and critical states, which are given by

$$E_c = \pm\lambda. \quad (3)$$

Before showing the rigorous proof, we present numerical verification. For this exactly solvable model, the different types of states can be identified by the fractal dimension (FD), defined for an arbitrary  $m$ -th eigenstate  $|\psi_m\rangle = \sum_{j=1}^L u_{m,j} a_j^\dagger |vac\rangle$  as  $FD = -\lim_{L \rightarrow \infty} \ln(\text{IPR})/\ln(L)$ , with the inverse participation ratio (IPR) being  $\text{IPR} = \sum_j |u_{m,j}|^4$ . The FD tends to 1 and 0 for the extended and localized states, respectively, while  $0 < FD < 1$  for critical states. Fig. 1(b) shows FD as a function of  $\lambda$  for different eigenstates of eigenvalues  $E$ . The dashed lines starting from band center denote the MEs  $E_c = \pm\lambda$ , across which FD changes from values close to 0.5 to values close to 0, indicating a critical-to-localization transition predicted by the analytic results. Particularly, we fix

$\lambda = 2.0$  and show FD of different eigenstates in Fig. 1(c) as a function of the corresponding eigenvalues for different sizes. The dashed lines in the figure are the MEs  $E_c = \pm\lambda = \pm 2.0$ . One can observe that the fractal dimension FD tends to 0 for all states in energy zones with  $|E| > \lambda$  with increasing the system size, implying that those states are localized. On the contrast, in energy zones with  $|E| < \lambda$ , the FD magnitude is far different from 0 and 1, and nearly independent of the system size.

*Rigorous proof.*—The above MEs and critical states can be analytically obtained by calculating the Lyapunov exponent (LE) in combination with zeros of hopping coefficients, which provides the unambiguous evidence of the critical zone. Denote by  $T_n(\theta)$  the transfer matrix of the Schrödinger operator, the LE can be computed via [57]

$$\gamma_\epsilon(E) = \lim_{n \rightarrow \infty} \frac{1}{n} \int \ln \|T_n(\theta + i\epsilon)\| d\theta,$$

where  $E$  is eigenvalue,  $\|T_n\|$  denotes the norm of matrix. By a standard complexification procedure [58], the LE is given by

$$2\gamma_\epsilon(E) = \max\{\ln |(|E| + \sqrt{E^2 - \lambda^2})/\lambda|, 0\}. \quad (4)$$

If  $|E| > |\lambda|$ ,  $2\gamma_0(E) = \ln |(|E| + \sqrt{E^2 - \lambda^2})/\lambda|$ , the state associated with  $E$  is localized with the localization length

$$\xi(E) = \frac{1}{\gamma_0} = \frac{2}{\ln |(|E| + \sqrt{E^2 - \lambda^2})/\lambda|}.$$

The eigenstates can either be extended or critical for  $\gamma_\epsilon = 0$  when  $|E| \leq |\lambda|$ , which belong to absolutely continuous (AC) spectrum or singular continuous (SC) spectrum, respectively [60]. There are two basic approaches to rule out the existence of AC spectrum (extended states), one is introducing unbounded spectrum [24] and the other is introducing zeros of hopping terms in Hamiltonian [61, 62]. For our model, there exists a sequence of sites  $\{2j_k\}$  such that  $t_{2j_k} \rightarrow 0$  in the thermodynamics limit, thus by [61] or Proposition 7.1 in [62], there is no AC spectrum (extended states), and the eigenstates associated with  $|E| \leq |\lambda|$  are all critical. In summary, vanishing LEs  $\gamma_\epsilon = 0$  and zeros of hopping coefficients altogether unambiguously determine the critical region for  $|E| \leq |\lambda|$  and positive LEs determine the localized region for  $|E| > |\lambda|$ . Therefore  $E = \pm\lambda$  mark critical energies separating localized states and critical states, manifesting MEs.

*Mechanism of critical states.*—The emergence of MEs and critical states has a universal underlying mechanism unveiled from the exact results. The existence of critical states is generated by zeros of hopping coefficients in the thermodynamic limit. Accompanied with zeros, those nearly zero hopping coefficients  $t_j$  effectively divide system into weakly coupled subchains, ruling out possibility of supporting extended states. Therefore eigenstates can only host either localized or critical states depending on the value of corresponding LEs. To further verify there is a plethora of critical states in the whole

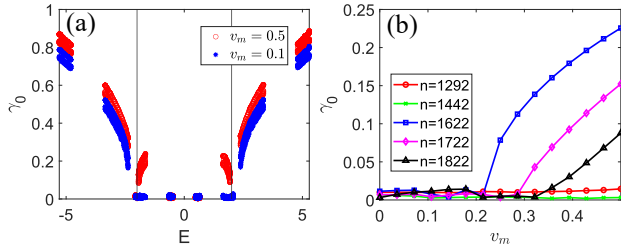


Figure 2. Numerical LEs  $\gamma_0$  for perturbation strength  $v_m$ . (a)  $\gamma_0$  of different eigenstates as a function of corresponding energies  $E$  for different  $v_m$ . Gray lines are original MEs. (b)  $\gamma_0$  as a function of  $v_m$  for eigenstates  $|\psi_n\rangle$  from the band center ( $n = 1292$ ) to the states nearby original MEs ( $n = 1822$ ). Critical states nearby MEs can be driven to localized states while critical zones nearby band center remains unchanged. The other parameters are  $\lambda = 2.0$  and  $L = 2584$ .

spectrum, let us consider first the special case with vanishing hopping coefficient  $\lambda \rightarrow 0$  [Fig. 1(a)]. In this case the model is divided into a series of dimmers, and each dimer renders a  $2 \times 2$  matrix with all elements being  $J_j = V_j = 2 \cos(2\pi\alpha j)$ . Then the eigenvalues are simply  $E_1 = 2J_j$  and  $E_2 = 0$ . Thus for  $\lambda = 0$ , the eigenstates have two classes. One is a class of localized states with nearly continuous spectrum  $E = 2J_j$ , and the other is a zero-energy flat band whose degeneracy equals to half of system size. Note that a linear combination of the zero modes are also eigenstates of the model, which can be either localized, extended or critical. Further inclusion of  $\lambda$  hybridizes the zero-energy flat-band modes and localized modes, yielding the critical states and MEs between them and localized ones. This mechanism also explains emergence of critical states starting from band center. Moreover, the number of critical states equals to that of localized states under the exactly solvable condition, since the degeneracy of flat band is half of system size, as verified by the numerical counting.

This zero hopping coefficients mechanism also explains a novel feature that the critical zone is robust against single-particle perturbation which tunes the model away from exactly solvable condition. We consider an extra mosaic on-site potential term  $V_p$  as perturbation, which represents the mismatch between mosaic hopping and onsite potentials in Hamiltonian given in Eq. (2), and is relevant to real experiment,

$$H_p = H + \sum_j V_j^p n_j, \quad (5)$$

where  $V_j^p = v_m \cos(2\pi\alpha j + \theta)$  for even- $j$  sites and  $V_j^p = v_m \cos[2\pi\alpha(j-1) + \theta]$  for odd- $j$  sites. Fig. 2 shows numerically calculated LEs for different  $v_m$ , with  $\lambda = 2$ . The sufficiently strong mismatch potentials can drive critical states nearby MEs into localized ones while for critical zones nearby the band center the states remains unchanged [Fig. 2(a)]. A more careful investigation of LEs shows that to drive critical states into localized ones requires finite  $v_m = v_m^c$ , with the magnitude  $v_m^c$  depending on the location of the critical state [Fig. 2(b)]. These results manifest the robustness of crit-

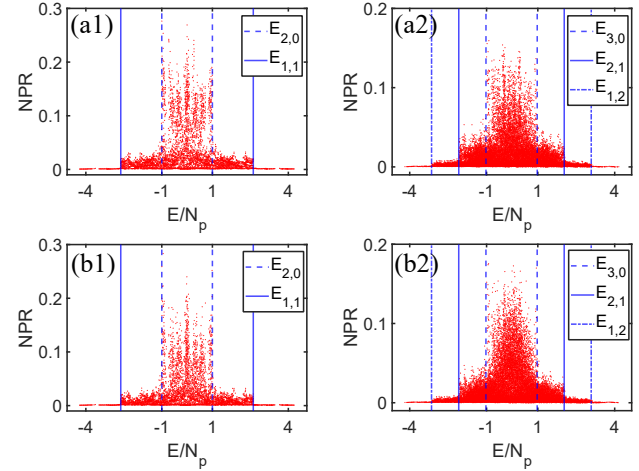


Figure 3. Normalized participation ratio (NPR) as a function of energy density  $E/N_p$  of few hardcore bosons case with  $U = 0$  (upper panel) and  $U = 1.4$  (lower panel), with  $\lambda = 1.0$  and  $t_0 = 1.0$ . Critical energy  $E_{c,l}$  is the maximal allowed energy  $c$  particles filled in critical orbitals and  $l$  particles filled in localized orbitals. (a1)(b1)  $N_p = 2$ ,  $L = 120$ . (a2)(b2)  $N_p = 3$ ,  $L = 60$ . The critical energy  $E_{2,0}(E_{3,0})$  is equal to the single particle ME  $E = \lambda$  for two (three) bosons case.

ical zones against perturbations, which is a key point of the present model. In comparison, the celebrated Aubry-André (AA) model exhibit a self-duality point at  $V = 2t$ , at which all states are critical [13]. However, those critical states are not robust and shall be quenched to localized state for infinitesimal perturbations. The present study unveils a generic mechanism to obtain robust critical zones protected by the zeros of hopping coefficients with vanishing LEs in the thermodynamic limit, which are not removed by the perturbations.

**Robustness against interactions.**—We further show the robustness of the MEs in the presence of interactions. We study a few-body Hamiltonian with hard-core bosons given by

$$H = H_0 + U \sum_j n_j n_{j+1}, \quad (6)$$

where  $H_0$  denotes the system with few hard-core bosons with Hamiltonian in Eq. (1), with  $\langle n_j \rangle \leq 1$ , and  $U$  denotes the strength of neighboring interactions between the hard-core bosons. This model can be simulated with Rydberg atoms (see details in next section). Our key prediction is that the MEs for the hard-core bosons with interactions are also robust. We examine the normalized participation ratio (NPR) [59] defined for each few-body eigenstate  $|\psi_m\rangle$  as  $\text{NPR} = 1/(\sum_{\{c\}} |u_{m,c}|^4 \times V_H)$ , where  $u_{m,c}$  is the wave function coefficient of eigenstate  $|\psi_m\rangle$  in the computational basis, and  $V_H$  is the size of Hilbert space. If the single-particle MEs are well defined in the presence of interaction, we shall observe three types of eigenstates resulted from particle filling [8, 9]. All the particles are filled into localized orbitals; all the particles are filled into critical orbitals and a mixed configuration with some particles filled into localized orbital while

others filled into critical orbital. The three types of states can be distinguished and characterized by NPR.

Fig. 3 shows NPR as a function of energy densities  $E/N_p$ , with  $N_p$  being the number of bosons for  $U = 0$  ( $= 1.4$ ) in upper (lower) panel. NPR displays a clear discontinuity at critical energy  $E_{c,l}$ , which is maximally allowed energy density for  $c$  particles filled in critical orbitals and  $l$  particles filled in localized orbitals. For example,  $E_{2,1}$  marks the maximal energy density for two particles filled in critical orbitals and one particle filled in localized orbital, in which one can detect such three-particle state if  $E/3 \in [-E_{2,1}, E_{2,1}]$ . It is interesting to find  $E_{c,l} = (c\lambda + lE_{\max})/N_p$ , with  $E_{\max}$  denoting the maximal energy density of the spectrum. Notice that in the single particle level,  $\lambda (E_{\max})$  is the maximal energy of critical (localized) orbitals, and  $E_{c,l}$  shows  $\lambda$  is still maximal energy of critical orbitals even in the presence of interactions. This indicates single particle MEs are still well defined in the presence of correlations, correlation only modifies energy distribution but does not shift the location of MEs, manifesting the robustness of MEs in the presence of interactions. This novel result motivates us to realize the exactly solvable model and observe our predictions with Rydberg atoms arrays [63–65] which are natural platforms to simulate hard-core bosons [66, 67].

**Experimental realization.**—Finally we propose an experimental scheme through an incommensurate Raman superarrays of Rydberg atoms [Fig. 4(a1)] to realize the model in Eq. (1). We show that the realization of Hamiltonian is precisely mapped to the realization of a two-leg lattice model, with even (odd) sites mapped to the sites on  $A(B)$ -leg as pictorially shown in Fig. 4(a2), whose Hamiltonian reads  $H = \sum_j (J_j a_j^\dagger b_j + \lambda a_j^\dagger b_{j+1} + \text{H.c.}) + \sum_j V_j (a_j^\dagger a_j + b_j^\dagger b_j)$ . The mapped Hamiltonian can be realized by Rydberg atoms based on three key ingredients. (i) AB-leg superarray with effective Zeeman splitting gradient applied along the  $x$  direction, (ii) two types of nearest neighbour couplings, with constant hopping coupling  $\lambda$  simulated by intrinsic dipolar interaction and quasi-periodic hopping coupling  $J_j$  induced by laser-assisted dipolar interaction, and (iii) the on-site incommensurate chemical potential  $V_j$ . Two Rydberg states  $|\downarrow\rangle = |70, S\rangle$  and  $|\uparrow\rangle = |70, P\rangle$  are chosen to simulate empty and occupied states of hard-core bosons at each site, with  $|0\rangle \equiv |\downarrow\rangle$  and  $|1\rangle \equiv |\uparrow\rangle$ . As indicated in Fig. 4(b1), the intrinsic dipole-dipole interactions between two Rydberg states lead to an exchange coupling, which can be mapped to constant hopping  $\lambda$  of the hard-core bosons [66, 67].

The AB-leg superarray and laser-assisted dipole-dipole interactions altogether realize incommensurate hoppings  $J_j$ . The inter-leg exchange couplings between same site are suppressed by the large energy detuning  $\Delta$ , but can be further restored by applying the Raman coupling potential  $V_R \propto \cos(4\pi\alpha j_x) \cos(\pi j_y) e^{i(\omega_2 - \omega_1)t} \sigma_{j_x, j_y}^x + \text{H.c.}$ , which is generated by two Raman beams with frequency difference  $\omega_1 - \omega_2 \approx \Delta$  such that the Zeeman splitting can be compensated by two-photon process [Fig. 4(b2)]. Furthermore, the spatial modulation of the Raman coupling potential determines the incommensurate strength of the induced exchange cou-

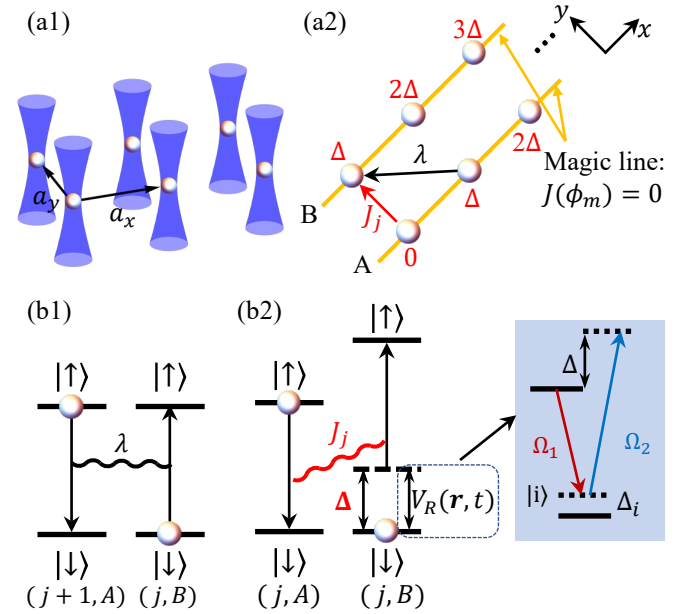


Figure 4. Realization of the quasiperiodic mosaic model in incommensurate Raman superarrays of Rydberg atoms. (a1) Rydberg atoms trapped in optical tweezers to form a two-leg array. (a2) The equivalent two-leg lattice model. The incommensurate and constant hopping coefficients are denoted as  $J_j$  and  $\lambda$ . An effective Zeeman splitting gradient (red) modifies energy difference between Rydberg states. The Rydberg atoms are tapped along the magic angle  $\phi_m$ , at which the amplitude of dipolar interaction vanishes. (b1) The intrinsic dipole-dipole interaction can induce constant hopping coupling  $\lambda$ . (b2) The exchange coupling between legs on the same site  $j$  is suppressed by the Zeeman detuning. A two-photon Raman process (see inset) compensates this energy penalty and induces the laser-assisted dipole-dipole interaction. The compensated exchange coupling realizes incommensurate hopping coupling  $J_j$ .

plings  $J_j = 2t_0 \cos 4\pi\alpha j$  (see Supplemental Material for details [58]). To prohibit laser-assisted exchange couplings along  $x$  direction, we use the angular dependence of dipole-dipole interaction  $V_{dd} = d^2(1 - 3\cos^2\phi)/R^3$  with  $d$  and  $R$  being the dipole moment and distance between two Rydberg levels, respectively. There exists a "magic angle"  $\phi_m = \arccos(1/\sqrt{3}) \approx 54.7^\circ$  [65, 68], along which the exchange coupling vanishes. By arranging the Rydberg atoms along the magic angle, we manage to prohibit hopping in the  $x$  direction. Finally, the incommensurate mosaic potential  $V_j$  can be realized via AC Stark shift [58]. Adding up those ingredients together and relabel the site index, we reach the model in Eq. (1). When a single hard-core boson is excited in this scheme, we can obtain the non-interacting critical states and MEs from the spectrum. Moreover, when several hard-core bosons are excited, critical energies depicted in Fig. 3 will be observed.

**Conclusion.**—We have proposed an exactly solvable 1D incommensurate mosaic models with experimental feasibility to realize new MEs separating localized states and critical states, and further proposed a novel experimental scheme us-

ing incommensurate Raman superarrays of Rydberg atoms for realization. By explicitly calculating the Lyapunov exponents (LEs), we have analytically obtained the expressions for MEs, which are in excellent agreement with the numerical studies. The robust critical states originates from a combination of zeros of hopping coefficients in the thermodynamic limit and zero LEs. We emphasize that these two features, serving as a generic mechanism to generate critical states, can be applied to construct a large class of analytical models hosting critical states. Our work broadens the concepts of MEs and provides a feasible lattice model that host exact MEs and unambiguous critical zones with experimental feasibility.

This work was supported by National Key Research and Development Program of China (2021YFA1400900 and 2020YFA0713300), the National Natural Science Foundation of China (Grants No. 11825401, No. 12261160368, No. 12071232, and No. 12061031). Q. Zhou was also supported by the Science Fund for Distinguished Young Scholars of Tianjin (No. 19JCJQJC61300) and Nankai Zhide Foundation.

\* These authors contribute equally to this work.

† [qizhou@nankai.edu.cn](mailto:qizhou@nankai.edu.cn)

‡ [xiongjunliu@pku.edu.cn](mailto:xiongjunliu@pku.edu.cn)

[1] P. W. Anderson, Absence of diffusion in certain random lattices, *Phys. Rev.* **109**, 1492 (1958).

[2] E. Abrahams, P. W. Anderson, D. C. Licciardello, and T. V. Ramakrishnan, Scaling Theory of Localization: Absence of Quantum Diffusion in Two Dimensions, *Phys. Rev. Lett.* **42**, 673 (1979).

[3] D. J. Thouless, Electrons in disordered systems and the theory of localization, *Phys. Rep.* **13**, 93 (1974).

[4] F. Evers and A. D. Mirlin, Anderson transitions, *Rev. Mod. Phys.* **80**, 1355 (2008).

[5] R. Whitney, Most Efficient Quantum Thermoelectric at Finite Power Output, *Phys. Rev. Lett.* **112**, 130601 (2014).

[6] C. Chiaracane, M. T. Mitchison, A. Purkayastha, G. Haack, and J. Goold, Quasiperiodic quantum heat engines with a mobility edge, *Phys. Rev. Research* **2**, 013093 (2020).

[7] K. Yamamoto, A. Aharony, O. Entin-Wohlman, and N. Hatano, Thermoelectricity near Anderson localization transitions, *Phys. Rev. B* **96**, 155201 (2017).

[8] X. Li, S. Ganeshan, J.H. Pixley, and S. Das Sarma, Many-Body Localization and Quantum Nonergodicity in a Model with a Single-Particle Mobility Edge, *Phys. Rev. Lett.* **115**, 186601 (2015).

[9] R. Modak and S. Mukerjee, Many-Body Localization in the Presence of a Single-Particle Mobility Edge, *Phys. Rev. Lett.* **115**, 230401 (2015).

[10] S. Nag and A. Garg, Many-body mobility edges in a one-dimensional system of interacting fermions, *Phys. Rev. B* **96**, 060203(R) (2017).

[11] F.A An, K. Padavić, E.J. Meier, S. Hegde, S. Ganeshan, J.H. Pixley, S. Vishveshwara, and B. Gadway, Interactions and Mobility Edges: Observing the Generalized Aubry-André Model, *Phys. Rev. Lett.* **126**, 040603 (2021).

[12] T. Kohlert, S. Scherg, X. Li, H. P. Lüschen, S. Das Sarma, I. Bloch, and M. Aidelsburger, Observation of Many-Body Localization in a One-Dimensional System with a Single-Particle Mobility Edge, *Phys. Rev. Lett.* **122**, 170403 (2019).

[13] S. Aubry and G. André, Analyticity breaking and Anderson localization in incommensurate lattices, *Ann. Israel Phys. Soc.* **3**, 133 (1980).

[14] S. Das Sarma, S. He, and X. C. Xie, Mobility edge in a model one-dimensional potential, *Phys. Rev. Lett.* **61**, 2144 (1988).

[15] D. J. Boers, B. Goedeke, D. Hinrichs, and M. Holthaus, Mobility edges in bichromatic optical lattices, *Phys. Rev. A* **75**, 063404 (2007).

[16] J. Biddle, B. Wang, D. J. Priour Jr, and S. Das Sarma, Localization in one-dimensional incommensurate lattices beyond the Aubry-André model, *Phys. Rev. A* **80**, 021603 (2009).

[17] J. Biddle and S. Das Sarma, Predicted mobility edges in one-dimensional incommensurate optical lattices: an exactly solvable model of Anderson localization, *Phys. Rev. Lett.* **104**, 070601 (2010).

[18] S. Ganeshan, J. H. Pixley, and S. Das Sarma, Nearest neighbor tight binding models with an exact mobility edge in one dimension, *Phys. Rev. Lett.* **114**, 146601 (2015).

[19] X. Deng, S. Ray, S. Sinha, G. V. Shlyapnikov, and L. Santos, One-dimensional quasicrystals with power-law hopping, *Phys. Rev. Lett.* **123**, 025301 (2019).

[20] X. Li, X. Li, and S. Das Sarma, Mobility edges in one dimensional bichromatic incommensurate potentials, *Phys. Rev. B* **96**, 085119 (2017).

[21] H. Yao, H. Khoudli, L. Bresque, and L. Sanchez-Palencia, Critical behavior and fractality in shallow one-dimensional quasiperiodic potentials, *Phys. Rev. Lett.* **123**, 070405 (2019).

[22] Y. Wang, X. Xia, L. Zhang, H. Yao, S. Chen, J. You, Q. Zhou, and X.-J. Liu, One dimensional quasiperiodic mosaic lattice with exact mobility edges, *Phys. Rev. Lett.* **125**, 196604 (2020).

[23] S. Roy, T. Mishra, B. Tanatar, and S. Basu, Reentrant Localization Transition in a Quasiperiodic Chain, *Phys. Rev. Lett.* **126**, 106803 (2021).

[24] T. Liu, X. Xia, S. Longhi, and L. Sanchez-Palencia, Anomalous mobility edges in one-dimensional quasiperiodic models, *SciPost Phys.* **12**, 027 (2022).

[25] J. Fraxanet, U. Bhattacharya, T. Grass, M. Lewenstein, and A. Dauphin, Localization and multifractal properties of the long-range Kitaev chain in the presence of an Aubry-André-Harper modulation, *Phys. Rev. B* **106**, 024204 (2022).

[26] Y. Wang, L. Zhang, S. Niu, D. Yu, X.-J. Liu, Realization and detection of non-ergodic critical phases in optical Raman lattice, *Phys. Rev. Lett.* **125**, 073204 (2020).

[27] J. Fraxanet, U. Bhattacharya, T. Grass, M. Lewenstein, and A. Dauphin, Localization and multifractal properties of the long-range Kitaev chain in the presence of an Aubry-André-Harper modulation, *Phys. Rev. B* **106**, 024204 (2022).

[28] Y. Wang, L. Zhang, W. Sun, T.-F J Poon, X.-J Liu Quantum phase with coexisting localized, extended, and critical zones, *arXiv:2202.06816*.

[29] G. Roati, C. D'Errico, L. Fallani, M. Fattori, C. Fort, M. Zaccanti, G. Modugno, M. Modugno, and M. Inguscio, Anderson localization of a non-interacting Bose-Einstein condensate, *Nature (London)* **453**, 895 (2008).

[30] H. P. Lüschen, S. Scherg, T. Kohlert, M. Schreiber, P. Bordia, X. Li, S. D. Sarma, and I. Bloch, Single-particle mobility edge in a one-dimensional quasiperiodic optical lattice, *Phys. Rev. Lett.* **120**, 160404 (2018).

[31] F. A. An, E. J. Meier, and B. Gadway, Engineering a flux-dependent mobility edge in disordered zigzag chains, *Phys. Rev. X* **8**, 031045 (2018).

[32] F. A. An, K. Padavić, E. J. Meier, S. Hegde, S. Ganeshan, J. H. Pixley, S. Vishveshwara, and B. Gadway, Observation of tunable

mobility edges in generalized Aubry-André lattices, *Phys. Rev. Lett.* **126**, 040603 (2021).

[33] Y. Wang, J.-H Zhang, Y Li, J Wu, W Liu, F Mei, Y Hu, L Xiao, J Ma, C Chin, and S Jia, Observation of Interaction-Induced Mobility Edge in an Atomic Aubry-André Wire, *Phys. Rev. Lett.* **129**, 103401 (2022).

[34] Y. Lahini, R. Pugatch, F. Pozzi, M. Sorel, R. Morandotti, N. Davidson, and Y. Silberberg, Observation of a localization transition in quasiperiodic photonic lattices, *Phys. Rev. Lett.* **103**, 013901 (2009).

[35] R. Merlin, K. Bajema, Roy Clarke, F. -Y. Juang, and P. K. Bhattacharya, Quasiperiodic GaAs-AlAs heterostructures, *Phys. Rev. Lett.* **55**, 1768 (1985).

[36] D. Tanese, E. Gurevich, F. Baboux, T. Jacqmin, A. Lemaître, E. Galopin, I. Sagnes, A. Amo, J. Bloch, and E. Akkermans, Fractal energy spectrum of a polariton gas in a Fibonacci quasiperiodic potential, *Phys. Rev. Lett.* **112**, 146404 (2014).

[37] V. Goblot, A. Štrkalj, N. Pernet, J. L. Lado, C. Dorow, A. Lemaître, L. Le Gratiet, A. Harouri, I. Sagnes, S. Ravets, A. Amo, J. Bloch and O. Zilberberg, Emergence of criticality through a cascade of delocalization transitions in quasiperiodic chains, *Nat. Phys.* **16**, 832 (2020).

[38] P. Roushan, C. Neill, J. Tangpanitanon, V.M. Bastidas, A. Megrant, R. Barends, Y. Chen, Z. Chen, B. Chiaro, A. Dunsworth, A. Fowler, B. Foxen, M. Giustina, E. Jeffrey, J. Kelly, E. Lucero, J. Mutus, M. Neeley, C. Quintana, D. Sank, A. Vainsencher, J. Wenner, T. White, H. Neven, D. G. Angelakis, J. Martinis, Spectroscopic signatures of localization with interacting photons in superconducting qubits, *Science* **358**, 6367 (2017).

[39] Y. Hatsugai and M. Kohmoto, Energy spectrum and the quantum Hall effect on the square lattice with nextnearest-neighbor hopping, *Phys. Rev. B* **42**, 8282 (1990).

[40] J. H. Han, D. J. Thouless, H. Hiramoto, and M. Kohmoto, Critical and bicritical properties of Harper's equation with next-nearest-neighbor coupling, *Phys. Rev. B* **50**, 11365 (1994).

[41] Y. Takada, K. Ino, and M. Yamanaka, Statistics of spectra for critical quantum chaos in one-dimensional quasiperiodic systems, *Phys. Rev. E* **70**, 066203 (2004).

[42] F. Liu, S. Ghosh, and Y. D. Chong, Localization and adiabatic pumping in a generalized Aubry-André-Harper model, *Phys. Rev. B* **91**, 014108 (2015).

[43] J. Wang, X.-J. Liu, X. Gao, and H. Hu, Phase diagram of a non-Abelian Aubry-André-Harper model with p-wave superfluidity, *Phys. Rev. B* **93**, 104504 (2016).

[44] T. Geisel R. Ketzmerick and G. Petschel, New class of level statistics in quantum systems with unbounded diffusion, *Phys. Rev. Lett.* **66**, 1651 (1991).

[45] K. Machida and M. Fujita, Quantum energy spectra and one-dimensional quasiperiodic systems, *Phys. Rev. B* **34**, 7367 (1986).

[46] C. L. Bertrand and A. M. García-García, Anomalous Thouless energy and critical statistics on the metallic side of the many-body localization transition, *Phys. Rev. B* **94**, 144201 (2016).

[47] T. C. Halsey, M. H. Jensen, L. P. Kadanoff, I. Procaccia, and B. I. Shraiman, Fractal measures and their singularities: The characterization of strange sets, *Phys. Rev. A* **33**, 1141 (1986).

[48] A. D. Mirlin, Y. V. Fyodorov, A. Mildenberger, and F. Evers, Exact Relations Between Multifractal Exponents at the Anderson Transition, *Phys. Rev. Lett.* **97**, 046803 (2006).

[49] R. Dubertrand, I. García-Mata, B. Georgeot, O. Giraud, G. Lemarié, and J. Martin, Two Scenarios for Quantum Multifractality Breakdown, *Phys. Rev. Lett.* **112**, 234101 (2014).

[50] H. Hiramoto and S. Abe, Dynamics of an electron in quasiperiodic systems. II. Harper's model, *J. Phys. Soc. Jpn.* **57**, 1365 (1988).

[51] R. Ketzmerick, K. Kruse, S. Kraut, and T. Geisel, What Determines the Spreading of a Wave Packet?, *Phys. Rev. Lett.* **79**, 1959 (1997).

[52] M. Larcher, F. Dalfovo, and M. Modugno, Effects of interaction on the diffusion of atomic matter waves in one-dimensional quasiperiodic potentials, *Phys. Rev. A* **80**, 053606 (2009).

[53] Y. Wang, C. Cheng, X.-J. Liu, and D. Yu, Many-body critical phase: extended and nonthermal, *Phys. Rev. Lett.* **126**, 080602 (2021).

[54] T. Xiao, D. Xie, Z. Dong, T. Chen, W. Yi, and B. Yan, Observation of topological phase with critical localization in a quasiperiodic lattice, *Science Bull.* **66**, 2175 (2021).

[55] A. Pal and D. A. Huse, Many-body localization phase transition, *Phys. Rev. B* **82**, 174411 (2010).

[56] R. Nandkishore and D. A. Huse, Many-body localization and thermalization in quantum statistical mechanics, *Annu. Rev. Condens. Matter Phys.* **6**, 15 (2015).

[57] A. Avila, Global theory of one-frequency Schrödinger operators, *Acta. Math.* **1**, 215 (2015).

[58] See Supplemental Material for details of the (i) finite size scalings, (ii) more perturbation results (iii) Lyapunov exponent, (iv) localization length and (v) experimental realizations, which includes Ref. [65, 69].

[59] S. Iyer, V. Oganesyan, G. Refael, and D. A. Huse, Many-body localization in a quasiperiodic system, *Phys. Rev. B* **87**, 134202 (2013).

[60] A. Avila, S. Jitomirskaya, and C. A. Marx, Spectral Theory of Extended Harper's Model and a Question by Erdős and Szekeres, *Invent. Math.* **210**, 283 (2017).

[61] Barry Simon and Thomas Spencer, Trace class perturbations and the absence of absolutely continuous spectra, *Commun. Math. Phys.*, 1989, **125**: 113-125.

[62] S. Jitomirskaya and C. A. Marx, Analytic quasi-periodic cocycles with singularities and the Lyapunov exponent of extended Harper's model, *Commun. Math. Phys.*, 2012, 316: 237-267.

[63] D. Barredo, S. de Léséleuc, V. Lienhard, T. Lahaye, and A. Browaeys, An atom-by-atom assembler of defect-free arbitrary two-dimensional atomic arrays, *Science* **354**, 1021 (2016).

[64] M. Endres, H. Bernien, A. Keesling, H. Levine, E. R. Anschuetz, A. Krajenbrink, C. Senko, V. Vuletic, M. Greiner, and M. D. Lukin, Atom-by-atom assembly of defect-free one-dimensional cold atom arrays, *Science* **354**, 1024 (2016).

[65] A. Browaeys and T. Lahaye, Many-body physics with individually controlled Rydberg atoms, *Nat. Phys.* **16**, 132 (2020).

[66] S. de Léséleuc, V. Lienhard, P. Scholl, D. Barredo, S. Weber, N. Lang, H. P. Büchler, T. Lahaye, and A. Browaeys, Observation of a symmetry-protected topological phase of interacting bosons with Rydberg atoms, *Science* **365**, 775 (2019).

[67] V. Lienhard, P. Scholl, S. Weber, D. Barredo, S. de Léséleuc, R. Bai, N. Lang, M. Fleischhauer, H. P. Büchler, T. Lahaye, and A. Browaeys, Realization of a Density-Dependent Peierls Phase in a Synthetic, Spin-Orbit Coupled Rydberg System, *Phys. Rev. X* **10**, 021031 (2020).

[68] S. Ravets, H. Labuhn, D. Barredo, T. Lahaye, and A. Browaeys, Measurement of the angular dependence of the dipole-dipole interaction between two individual Rydberg atoms at a Förster resonance, *Phys. Rev. A* **92**, 020701(R) (2015).

[69] T.-H Yang, B.-Z Wang, X.-C Zhou, and X.-Jun Liu, Quantum Hall states for Rydberg arrays with laser-assisted dipole-dipole interactions, *Phys. Rev. A* **106**, L021101 (2022).

## Supplementary Material

This Supplemental Material provides additional information for the main text. In Sec. S-1, we perform the finite size analysis for the FD. In Sec. S-2, we present other forms of perturbation potentials and other values of  $\lambda$  in few-body calculations. In Sec. S-3, we give the details of computing Lyapunov exponent, and the numerical results of localization length are shown in Sec. S-4. Finally, we give details of experimental realization in Sec. S-5.

### S-1. FINITE SIZE SCALINGS

In this section, we study the finite size scaling of eigenstates by calculating FD of two typical eigenstates. As mentioned in main text, the FD tends to 1 and 0 for the extended and localized states, respectively, and  $0 < \text{FD} < 1$  for critical states. Fig. S1 (a) and (b) show the FD of the eigenstates corresponding to the bottom and center of the spectrum, which are typical eigenstates for the localized and critical orbitals, respectively. It is observed that FD tends to 0 for the lowest eigenstates, and tends to finite value between 0 and 1 for the center states of the spectrum.

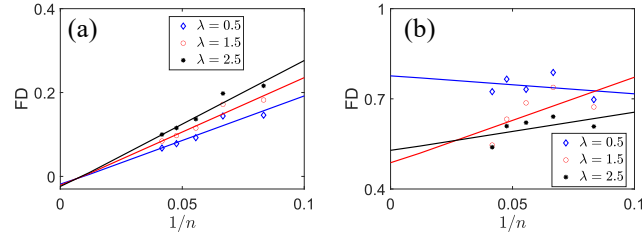


Figure S1. FD as a function of  $1/n$  for (a) the lowest state and (b) center state of the spectrum for different  $\lambda$ . Here  $n$  is the index of Fibonacci numbers  $F_n$ .

### S-2. MORE PERTURBATION RESULTS

In the main text, we have showed that the critical zone is robust against experimentally relevant perturbation and is also against interactions between particles. To further demonstrate robust critical zone is indeed protected by zeros of hopping coefficients, we present more numerical results of perturbations, although the forms of perturbative terms are not physically relevant. In this section, the on-site perturbation  $V_p$  is given by

$$V_p = v_p \sum_j \cos(2\pi m\alpha j + \phi) n_j, \quad (\text{S1})$$

and the hopping perturbation  $T_p$  is given by

$$T_p = t_p \sum_j [\cos(2\pi m\alpha j + \phi) b_j^\dagger b_{j+1} + \text{H.c.}], \quad (\text{S2})$$

with  $m \in \mathbb{Z}$  and here we choose  $m = 3$ . Fig. S2 shows FD of eigenstates as a function of energies  $E$  and strength of perturbations and interactions. Similar to the results in the main text, the critical zone is robust against moderate perturbation as expected. It is observed that adding perturbative hopping term is easier to drive system into localized phase compared to adding perturbative on-site term. This is because  $T_p$  directly acts on the hopping terms and is easier to remove the zeros of hopping coefficients compared to the on-site perturbation  $V_p$ . Another feature is that a second ME emerges due to perturbations, and the localization transitions start from center of the spectrum instead of edge of the spectrum. One can introduce more terms as perturbation and choose  $m$  as arbitrary integer and will obtain similar results, indicating robustness of the MEs protected by the generic mechanism.

We also present more numerical results of robustness against interactions. For the case  $\lambda = 2$ ,  $t_0 = 1$  and  $V = 1.4$ , the critical energy is less prominent compared with the results in the main text, but the relation  $E_{c,l} = (c\lambda + lE_{\max})$  still holds and single particle ME still exists as illustrated in Fig. S2(b).

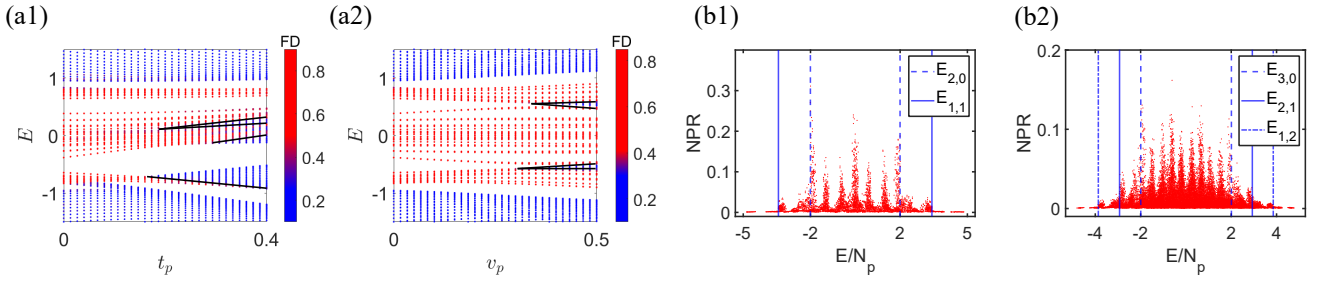


Figure S2. Fractal dimension (FD) of different eigenstates as a function of corresponding energies  $E$  and (a1) strength of perturbative hopping term  $t_p$  and (a2) perturbative on-site potential  $v_p$ . New MEs are marked by black lines. Other parameters are  $\lambda = 0.8$  and  $L = 2584$ . And Normalized participation ratio (NPR) as a function of energy density  $E/N_p$  of few hardcore bosons case with nearest neighbor interaction  $U = 1.4$ , with  $\lambda = 2.0$ ,  $t_0 = 1.0$  and (b1)  $N_p = 2$ ,  $L = 120$  (b2)  $N_p = 3$ ,  $L = 60$ . The critical energy  $E_{2,0}(E_{3,0})$  is equal to the single particle ME  $E = \lambda$  for two (three) bosons case.

### S-3. LYAPUNOV EXPONENT

In this section, we give a detailed derivation of Lyapunov exponent of the proposed model. We let  $t_0 = 1$  for simplicity. For an irrational  $\alpha$ , consider the quasiperiodic Jacobi operators on  $l^2(\mathbb{Z})$ ,

$$(H_{\lambda, \alpha, \theta} \psi)_n := V_n \psi_n + t_n \psi_{n+1} + \bar{t}_{n-1} \psi_{n-1}, \quad \theta \in \mathbb{T}, \quad \lambda \neq 0. \quad (\text{S3})$$

Where

$$V_n(\theta) = \begin{cases} 2 \cos[2\pi(n-1)\alpha + \theta], & n = 1, \quad \text{mod } 2, \\ 2 \cos(2\pi n \alpha + \theta), & n = 0, \quad \text{mod } 2, \end{cases}$$

and

$$t_n(\theta) = \begin{cases} \lambda, & n = 1, \quad \text{mod } 2, \\ 2 \cos(2\pi n \alpha + \theta), & n = 0, \quad \text{mod } 2. \end{cases}$$

Denote by  $T_n(\theta)$  the transfer matrix of the Jacobi operator, then LE can be computed as

$$\gamma_\epsilon(E) = \lim_{n \rightarrow \infty} \frac{1}{n} \int \ln \|T_n(\theta + i\epsilon)\| d\theta,$$

where  $\|A\|$  denotes the norm of the matrix  $A$ . First note that the transfer matrix can be written as

$$\begin{aligned} T_2(\theta) &= \frac{1}{2\lambda \cos(2\pi\alpha + \theta)} \begin{pmatrix} E - 2\cos(2\pi\alpha + \theta) & -2\cos(2\pi\alpha + \theta) \\ \lambda & 0 \end{pmatrix} \begin{pmatrix} E - 2\cos(2\pi\alpha + \theta) & -\lambda \\ 2\cos(2\pi\alpha + \theta) & 0 \end{pmatrix}, \\ &= \frac{1}{2\lambda \cos(2\pi\alpha + \theta)} \begin{pmatrix} E^2 - 4E\cos(2\pi\alpha + \theta) & -\lambda E + 2\lambda \cos(2\pi\alpha + \theta) \\ \lambda E - 2\lambda \cos(2\pi\alpha + \theta) & -\lambda^2 \end{pmatrix}. \end{aligned}$$

Consider a new matrix

$$\begin{aligned} \tilde{T}_2(\theta) &:= 2\lambda \cos(2\pi\alpha + \theta) T_2(\theta), \\ &= \begin{pmatrix} E^2 - 4E\cos(2\pi\alpha + \theta) & -\lambda E + 2\lambda \cos(2\pi\alpha + \theta) \\ \lambda E - 2\lambda \cos(2\pi\alpha + \theta) & -\lambda^2 \end{pmatrix}, \end{aligned}$$

we denote by  $\tilde{\gamma}_\epsilon(E)$  the corresponding Lyapunov exponent, and it is continuous about  $\epsilon$  since  $\tilde{T}_2(\theta)$  is analytic. Thus

$$\gamma_\epsilon(E) = \tilde{\gamma}_\epsilon(E) - \frac{1}{2} \int \ln |2\lambda \cos(\theta + i\epsilon)| d\theta = \tilde{\gamma}_\epsilon(E) - \frac{1}{2} \ln |\lambda| - \pi|\epsilon|, \quad (\text{S4})$$

which means  $\gamma_\epsilon(E)$  is continuous about  $\epsilon$ . Let us complexify the phase of  $T_2(\theta)$ , and let  $\epsilon$  goes to infinity, direct computation yields

$$T_2(\theta + i\epsilon) = \frac{1}{\lambda} \begin{pmatrix} -2E & \lambda \\ -\lambda & 0 \end{pmatrix} + o(1).$$

Thus we have

$$\gamma_\epsilon(E) = \frac{1}{2} \ln \left| \frac{|E| + \sqrt{E^2 - \lambda^2}}{\lambda} \right| + o(1).$$

If  $\epsilon > 0$  is large enough, Avila's global theory shows that, as a function of  $\epsilon > 0$ ,  $2\gamma_\epsilon(E)$  is a convex, piecewise linear function, and their slopes are integers multiply  $2\pi$ . Furthermore,  $\gamma_\epsilon(E)$  is continuous about  $\epsilon$ , which implies that

$$\gamma_\epsilon(E) = \frac{1}{2} \max \left\{ \ln \left| \frac{|E| + \sqrt{E^2 - \lambda^2}}{\lambda} \right|, 0 \right\}.$$

So we obtain the LE in the main text.

#### S-4. LOCALIZATION LENGTH

In this section, we numerically verify the localization length  $\xi$  obtained in the main text. As shown in Fig. S3, the red lines represent  $|\psi|_{\max} \exp(-|i - i_0|/\xi)$ , where  $|\psi|_{\max}$  is the maximum values of  $|\psi|$  in the two peaks,  $i_0$  is the corresponding lattice sites and  $\xi$  is the localization length which is given by  $\xi(E) = 2/\ln[|E| + \sqrt{E^2 - \lambda^2}/|\lambda|]$ . It is indicated the analytical expressions of the localization length  $\xi$  well describe the localization features of the corresponding eigenstates.

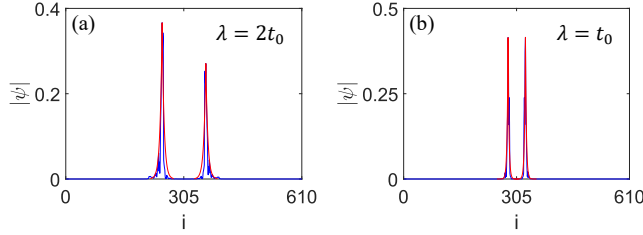


Figure S3. Spatial distributions of eigenstates. Blue lines represent  $|\psi|$ , where  $\psi$  is the eigenstates corresponding to (a)  $E = -2.1(6)t_0$  with  $\lambda = 2t_0$ , (b)  $E = -1.3(5)t_0$  with  $\lambda = t_0$ . Here we fix  $L = 610$ . The red lines represent  $|\psi|_{\max} \exp(-|i - i_0|/\xi)$ .

#### S-5. EXPERIMENTAL REALIZATION

In this section, we illustrate how to realize the lattice model in the main text. Our basic idea is to use well-tuned Rydberg atoms to simulate hard-core bosons with hoppings and on-site potentials controlled by external fields. We shall realize the Hamiltonian

$$H = \sum_{j_x} (J_{j_x} \sigma_{j_x, A}^+ \sigma_{j_x, B}^- + \lambda \sigma_{j_x, A}^+ \sigma_{j_x+1, B}^- + \text{H.c.}) + \frac{1}{2} \sum_{j_x, s=\{A, B\}} V_{j_x} (\mathbb{1} + \sigma_{j_x, s}^z), \quad (\text{S5})$$

which can be transformed into the model (1) by relabeling site index  $j_x \rightarrow 2j - 1$  for  $j_x$  on A-leg and  $j_x \rightarrow 2j$  for  $j_x$  on B-leg, and defining bosonic operator  $b_j^\dagger = |1\rangle_j \langle 0|_j$  at each site, with  $|1\rangle \equiv |\uparrow\rangle$  and  $|0\rangle \equiv |\downarrow\rangle$ . In the following we shall take  $^{87}\text{Rb}$  atoms as an example. For  $^{87}\text{Rb}$ , two Rydberg states are chosen to simulate spin 1/2 at each site with  $|\downarrow\rangle \equiv |70, S\rangle$  and  $|\uparrow\rangle \equiv |70, P\rangle$ . We consider the two-leg superarray of Rydberg atoms, with each trapped in optical tweezers. We consider the two-leg superarray of Rydberg atoms, with each trapped in optical tweezers. An effective Zeeman splitting  $M_{j_x, s}$  is introduced along the  $x$  direction, with  $M_{j_x+1, s} - M_{j_x, s} = \Delta$ ,  $M_{j_x=0, A} = 0$  and  $M_{j_x=0, B} = 0$ . Three Raman beams are applied to generate Raman and AC Stark potential. The total Hamiltonian of the system is given by,

$$H = H_{\text{dipole}} + H_{\text{Zeeman}} + V_R(\mathbf{r}, t) + V_{\text{AC}}(\mathbf{r}), \quad (\text{S6})$$

which includes the bare dipole-dipole interactions [S1]

$$H_{\text{dipole}} = \sum_{j_x} J_y^0 \sigma_{j_x, A}^+ \sigma_{j_x, B}^- + J_d^0 \sigma_{j_x-1, A}^+ \sigma_{j_x, B}^- + \sum_{|i-j|>1} \frac{J_{ij}}{R_{ij}^3} \sigma_{i, A}^+ \sigma_{j, B}^- + \text{H.c.},$$

with  $J_y^0 = C_3/a_y^3$  and  $J_d^0 = C_3/(a_x^3 + a_y^3)^{3/2}$ , the effective Zeeman energy gradient term,

$$H_{\text{Zeeman}} = \frac{1}{2} \sum_{j_x, s=\{A, B\}} M_{j_x, s} \sigma_{j_x, s}^z,$$

the Raman coupling potential obtain from time-dependent perturbation [S2]

$$V_R(\mathbf{r}, t) = \frac{\Omega_1(\mathbf{r}, t)^* \Omega_2(\mathbf{r}, t)}{\Delta_i} \sigma_{j_x, j_y}^x,$$

and the AC Stark term

$$V_{\text{AC}}(\mathbf{r}) = \frac{|\Omega_3(\mathbf{r})|^2}{\Delta'_i}.$$

As discussed in the main text, the bare dipole-dipole interactions between Rydberg states with the same Zeeman energy constitute the constant hopping coupling  $\lambda = J_d^0$ . In the following, we discuss the scheme for realizing the incommensurate hopping couplings and on-site potential.

### A. The incommensurate hoppings

The incommensurate hoppings are simulated by laser-assisted dipole-dipole interactions. The bare dipole-dipole interactions between legs on the same  $j_x$  are suppressed by the large Zeeman splitting  $\Delta$ , but can be further restored by applying the Raman coupling potential  $V_R$ . The Raman coupling potential is generated by two Raman lights with Rabi-frequencies  $\Omega_{1,2}$  and the frequencies  $\omega_{1,2}$ . When the frequency difference satisfies nearly resonant condition  $\omega_1 - \omega_2 \approx \Delta$ , then the Zeeman detuning  $\Delta$  is compensated by the two-photon process. Here we choose  $\Omega_1 = \Omega_0 \cos(2\pi\alpha j_x + \frac{\pi}{4}) e^{i\theta_1}$  and  $\Omega_2 = \Omega_0 \sin(2\pi\alpha j_x + \pi j_y + \frac{\pi}{4}) e^{i\theta_2}$ , direct calculation yields the Raman potential

$$V_R(\mathbf{r}, t) = \sum_{j_x, j_y} \frac{|\Omega_0|^2}{2\Delta_i} \cos(4\pi\alpha j_x) \cos(\pi j_y) e^{i\delta\theta} \sigma_{j_x, j_y}^x + \text{H.c.}, \quad (\text{S7})$$

with  $\delta\theta = \theta_2 - \theta_1$ . So we choose  $\theta_2 = \theta_1 + n\pi$ , which can be realized in experiment. To the lowest order, the effective exchange couplings are [S2]

$$J_{j_x} = \frac{|\Omega_0|^2}{\Delta\Delta_i} \cos(2\pi\alpha j_x) J_y^0, \quad (\text{S8})$$

which realize the incommensurate hopping coefficients. Notice that the transition between  $j_x$  and  $j_x + 2$  and longer distance are suppressed by larger Zeeman energy offset (i.e., at least  $2\Delta$ ) and cannot be induced by two-photon process. To prohibit laser-assisted exchange coupling within the same leg, we use the angular dependence of dipole-dipole interaction  $J = d^2(3\cos^2\theta_{ij} - 1)/R_{ij}^2$  as discussed in the main text. We arrange the Rydberg atoms along the "magic angle"  $\theta_m = \arccos(1/\sqrt{3}) \approx 54.7^\circ$ , at which the dipolar interactions vanish. So there is no hopping coupling generated by Raman potential along the  $x$  direction.

### B. The incommensurate on-site potential

We apply another standing wave field to generate an incommensurate on-site potential  $V_{\text{AC}}(\mathbf{r})$ , which is  $\Omega_3(\mathbf{r}) = \Omega'_0 \cos(2\pi\alpha j_x)$ . Together with an additionally correction from Raman potential, the total on-site term is given by

$$\begin{aligned} V_{\text{on-site}} &= \frac{|\Omega_1|^2 + |\Omega_2|^2}{\Delta_i} + V_{\text{AC}} \\ &= \frac{1}{\Delta_i} \left[ |\Omega_0|^2 \cos^2(2\pi\alpha j_x + \frac{\pi}{4}) + |\Omega_0|^2 \sin^2(2\pi\alpha j_x + \pi j_y + \frac{\pi}{4}) \right] + \frac{1}{\Delta'_i} [|\Omega'_0|^2 \cos^2(2\pi\alpha j_x)] \\ &= \frac{|\Omega_0|^2}{\Delta_i} + \frac{|\Omega'_0|^2}{2\Delta'_i} + \frac{|\Omega'_0|^2}{2\Delta'_i} \cos(4\pi\alpha j_x), \end{aligned} \quad (\text{S9})$$

of which the constant part can be neglected and we can reach the desired on-site incommensurate potential.

### C. Experimental parameters

Here, we also give an estimate of the orders of magnitude of the relevant experimental parameters. The data given here are based on  $^{87}\text{Rb}$  atoms. For the states  $|70S\rangle$  and  $|70P\rangle$ ,  $C_3 = 4196\text{MHz} \cdot \mu\text{m}^{-3}$ . Then with  $a_y/a_x = 0.8$ ,  $|\Omega_0| = |\Omega'_0| = 200\text{MHz}$ ,  $\Delta = 10\text{MHz}$  and  $\Delta_i = 16.5\text{Ghz}$  and  $a_x = 12.5\mu\text{m}$ , we obtain the model with  $t_0 = |\Omega_1\Omega_2 J_y^0/(2\Delta\Delta_i)| = 0.5\text{ MHz}$ ,  $\lambda = 1\text{MHz}$

To observe the correlated effects, the lifetime of the system should be large compared to the characteristic time of the system. For  $\lambda = 1\text{MHz}$ , a lifetime of at least  $\tau > \tau_0 = 100J_0^{-1} = 100\mu\text{s}$  is needed. The lifetime of the Rydberg states  $|70S\rangle$  and  $|70P\rangle$  are  $370\mu\text{s}$  and  $750\mu\text{s}$  respectively. The lifetime of  $6P$  states, which the Raman process coupled, has a lifetime of  $\tau_{6P} = 130\text{ns}$ . So for the single photon detuning  $\Delta_i = 16.5\text{ GHz}$  and  $\Delta'_i = 20\text{ GHz}$ , the lifetime can be estimated by  $\tau = (2|\Omega_0|/\Delta_i + |\Omega'_0|/\Delta'_i)^{-2} \tau_{6P} \approx 110\mu\text{s} > \tau_0$ .

---

\* These authors contribute equally to this work.

† [qizhou@nankai.edu.cn](mailto:qizhou@nankai.edu.cn)

‡ [xiongjunliu@pku.edu.cn](mailto:xiongjunliu@pku.edu.cn)

[S1] A. Browaeys and T. Lahaye, Many-body physics with individually controlled Rydberg atoms, *Nat. Phys.* **16**, 132 (2020).

[S2] T.-H Yang, B.-Z Wang, X.-C Zhou, and X.-Jun Liu, Quantum Hall states for Rydberg arrays with laser-assisted dipole-dipole interactions, *Phys. Rev. A* **106**, L021101